Progress In Electromagnetics Research Letters, Vol. 107, 27–32, 2022

Power Absorption of 3D Printed Layers on a Microstrip Line

Chung-Yen Hsu and Lih-Shan Chen*

Abstract—Power-absorbing layers on a microstrip line prepared by 3D printing are investigated in this study. Polylactic acid (PLA) with added carbon is used in the 3D printing process for the preparation of the power-absorbing layers. The S-parameters of the 3D-printed layers are measured using a vector network analyzer. The effect of the layer thicknesses on the power absorption which enables high-frequency devices to function correctly is discussed. As the layer thickness increases, the magnitude of S_{11} increases while the magnitude of S_{21} decreases accordingly. The experimental results show that the power absorption is within 80–95% (sheet resistance: 75.1 Ω/□–823.76 Ω/□), in the frequency range of 2–6 GHz. In addition, simulated S-parameter analysis was performed using a high-frequency structure simulator. The simulation results are in good agreement with the experimental results.

1. INTRODUCTION

High-frequency unwanted electromagnetic interference (EMI) from signal transmission lines or electromagnetic waves affects the performance of electronic systems. EMI comprises conducted emission (CE) and radiated emission (RE), while electromagnetic susceptibility (EMS) includes conducted susceptibility (CS) and radiated susceptibility (RS) [1]. Many types of magnetic or non-magnetic films on a microstrip line have been proposed [2–5] for power absorption. Various techniques such as RF magnetron co-sputtering, metal-organic chemical vapor deposition, and pulsed laser deposition have been used to fabricate power absorption films. Other methods for power absorption include the use of shield gaskets [6] and filters [7, 8] for absorbing the power from RF. In recent years, 3D printing technology has experienced significant progress and is now available in various fields. The fused deposition modeling (FDM) printing technique is used with commercial materials like acrylonitrile butadiene styrene (ABS) or polylactic acid (PLA) for realizing different thicknesses, patterns and composite materials. An internal mesh layer with a varying conductive polymer volume content fabricated using the 3D printing process was prepared for EMI shielding structures [9]. The electromagnetic shielding performance of the 3D-printed polymer composites in the C-band of the electromagnetic spectrum (3.5–7.0 GHz) was investigated [10]. In [11] PLA-based composite materials were adopted as microwave circuit-analog (CA) absorbers. Prototype absorbers with approximately a $0.1\lambda_0$ thickness exhibited 20 dB of absorption at the resonant frequencies. In [12], polylactic acid was used as a dielectric material and a conductive pattern was realized by applying silver paste to the 3-D printed dielectric structure and preparing miniaturized metamaterial absorbers. Noise suppression at gigahertz high frequency is required in printed circuit board and in an RF transmission line. In our previous study the power absorption characteristics of films on a microstrip line prepared by spin coating and screen printing were investigated [13, 14]. In this work, 3D printing process was used to prepare the power absorption layers on a microstrip line. The absorption of power by 3D printed technology was evaluated and the S-parameters and ratio of power loss (P_{loss}) to input power (P_{in}) are discussed. In addition, the experimental results are compared with the simulation results obtained using a high-frequency structure simulator (HFSS).

Received 5 August 2022, Accepted 14 October 2022, Scheduled 17 October 2022
* Corresponding author: Lih-Shan Chen (lschen@isu.edu.tw).
The authors are with the Department of Electronic Engineering, I-Shou University, Taiwan.

2. FABRICATION

The 3D printing material used to create layers on an FR4 substrate is commercially available electrically conductive PLA CDP11701 (manufactured by Proto-Pasta) [15]. CDP11701 is a composite of a carbon black conductive fiber and a polylactide resin, which has the advantages of good adhesion and a high melt flow rate. The 3D printing equipment ANET A6 is employed for pouring PLA over the layers in different thicknesses. The parameter settings for 3D printing are listed in Table 1.

Table 1. Anet-A6 3d printing parameter settings.

No.	Parameter	Level
1	Print temperature (°C)	180
2	Height of deposition (mm)	0.1
3	Printing speed (mm/s)	60
4	Travel speed (mm/s)	120
5	Heated bed temperature (°C)	60

The 3D printed power-absorbing layer is located in the central part of the transmission line (40 mm × 3 mm) on an FR4 substrate. The FR4 substrate has a thickness of 1.6 mm, a dielectric constant ε_r of 4.4 and a loss tangent of 0.02. The power-absorbing layer has dimensions of 40 mm × 30 mm and different thicknesses ranging from 0.2 to 2 mm, as shown in Figure 1. In this study, Mitutoyo Digimatic micrometers with a range of 25.4 mm and a resolution of 0.001 mm are employed for measuring the thicknesses of the 3D printed layers. A vector network analyzer, E5080B VNA (KEYSIGHT), is employed for S-parameter (return loss and insertion loss) measurements, and full two-port SOLT calibration is used to perform 85052D 3.5 mm mechanical calibration. Simulated S-parameter analysis of the microstrip line with or without 3D printed layers was performed using an HFSS (Ver. 11.1.3, Ansoft Co.).

3. RESULTS AND DISCUSSION

The sheet resistances of 3D-printed layers with different thicknesses are listed in Table 2. The expected thickness of 3D printed layers is chosen to obtain an extensive range of sheet resistances. The expected thickness ranges from 0.2 mm to 2 mm while the measured thickness ranges from 0.182 mm to 1.981 mm, as listed in Table 2. The value of the electrical conductivity of the 3D-printed material (PLA CDP11701) which is 6.67 S/m is used in the calculation of the sheet resistance. The sheet resistance (Rs) of the 3D-printed specimens is inversely proportional to the layer thickness (t) and is calculated using $Rs = 1/(\sigma * t)$, where σ is the conductivity. The sheet resistance decreases from 823.76/□ to 75.71 Ω/□ with an increase in the thickness from 0.182 mm to 1.981 mm, as listed in Table 2.

Table 2. Sheet resistance of 3D printed specimens with different thicknesses.

Expected Thickness (mm)	0.2	0.5	1	2
Measured Thickness (mm)	0.182	0.470	0.986	1.981
Conductivity (S/m)	6.67	6.67	6.67	6.67
Rs (Ω/□)	823.76	318.98	152.05	75.71

The injected microwave power includes the reflected, transmitted, and absorbed powers. The reflected and transmitted powers are calculated from S_{11} and S_{21} given in Eqs. (1) and (2), respectively. The absorbed power is defined by the ratio of the power loss (P_{loss}) to the input power (P_{in}) of the

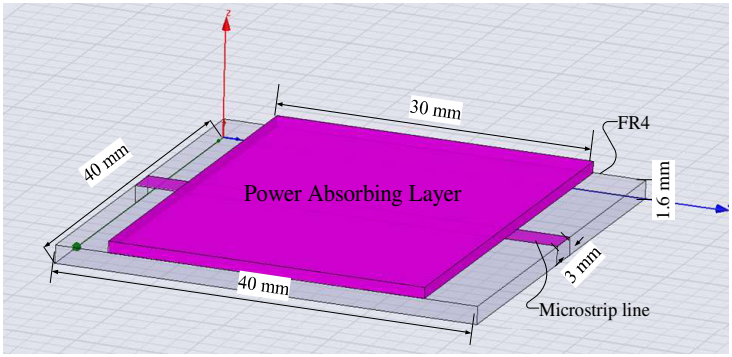

(a)

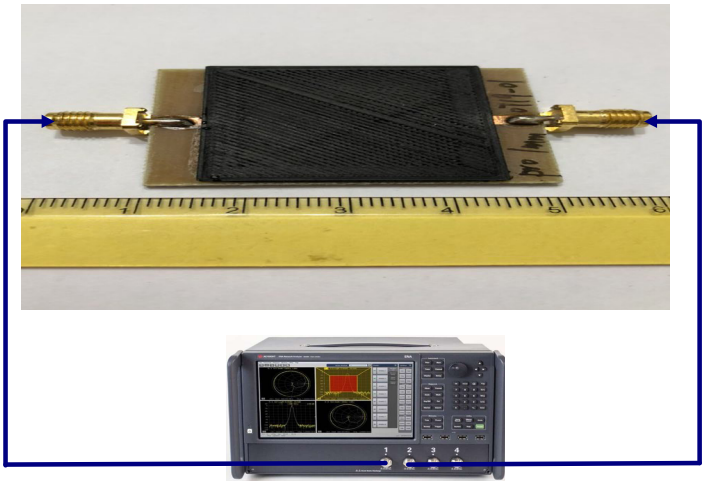

(b)

Figure 1. Structure of 3D-printed layer on microstrip line. (a) Power absorbing layer on microstrip line, (b) using vector network analyzer S parameters.

layers on the microstrip line, as represented in Eq. (3).

$$S_{11} = 20\log|\Gamma| \tag{1}$$

$$S_{21} = 20\log|T| \tag{2}$$

$$P_{loss}/P_{in} = 1 - |S_{11}|^2 - |S_{21}|^2 \tag{3}$$

The magnitude of S_{11} for specimens without a 3D-printed layer is rather small, indicating less reflection in the microstrip line, as shown in Figure 2. However, the attachment of a 3D-printed layer onto the microstrip line changes the characteristic impedance of the transmission line. As the layer thickness grows from 0.182 mm to 1.981 mm, the magnitude of S_{11} increases and moves towards the value of 0 dB. An increase in the layer thickness results in a higher wave reflection in the microstrip line due to an increased impedance mismatch at the boundary of the power absorption layer.

Figure 3 shows the frequency dependence of S_{21} for 3D-printed specimens with an increasing thickness from 0.182 mm to 1.981 mm. The magnitude of S_{21} for specimens without a 3D printed layer decreases slightly with the frequency from a value of 0 dB which shows highly transmitting characteristics. With an increase in the 3D printed layer thickness, the magnitude of S_{21} decreases. The transmission signal attenuation at a frequency of 6 GHz shifts from -8 dB to -19 dB while the layer thickness increases from 0.182 mm to 1.981 mm, as shown in Figure 3. In comparison with the values in Figure 2 and Figure 3, the magnitude of S_{11} increases with an increase in the layer thickness, while the magnitude of S_{21} decreases accordingly.

As there is a small gap between the microstrip line and the 3D printed layer, a strong capacitance is formed, and a current is induced in the 3D printed layer by an electrical field from the microstrip

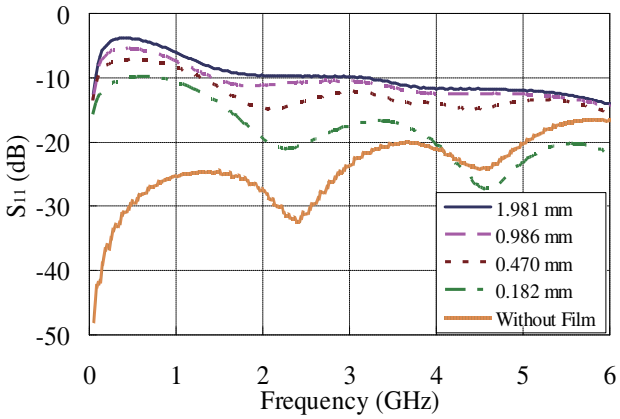

Figure 2. Frequency dependence of S_{11} for 3D printed layers with different thicknesses.

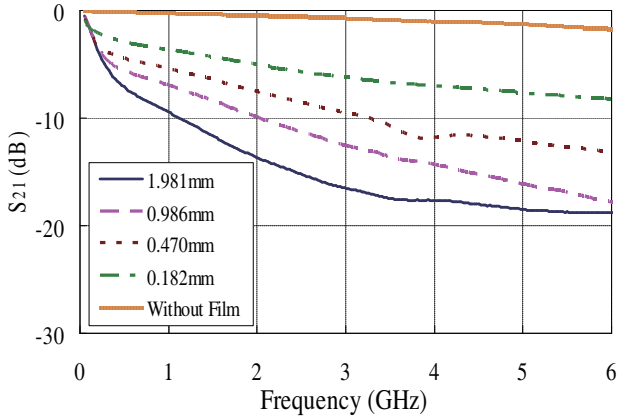

Figure 3. Frequency dependence of S_{21} for the 3D-printed layers with different thicknesses.

line. When the electromagnetic wave signal reaches the 3D printed layer on the microstrip line, the power loss mechanism consists of ohmic loss through the electric field around the microstrip line. Power absorption by ohmic loss is expressed by Eq. (4) [2]

$$P = \frac{1}{T}\int_{t}^{t+T} \sigma \int_{\Delta V} E^2 dV dt \tag{4}$$

where T is the time of one cycle, σ the electrical conductivity, E the electric field strength, and V the volume of the 3D printed layer. According to Eq. (4), at a given electrical conductivity, the ohmic power loss is proportional to the layer thickness. Therefore, when the 3D printed layer thickness is increased, ohmic power loss increases and the magnitude of S_{21} decreases, as shown in Figure 3.

Different 3D printed layer thicknesses result in different power absorptions (P_{loss}/P_{in}), as shown in Figure 4. The P_{loss}/P_{in} value increases as the measured frequency increases. In addition, the P_{loss}/P_{in} value of the thicker layer (lower sheet resistance) is higher than that of the thinner layer (higher sheet resistance) measured at the same frequency. We observed that the specimens with a 0.470 mm layer thickness (corresponding to 318.98 Ω/□) exhibited a power absorption (P_{loss}/P_{in}) of 80% at 2 GHz. Simulation and experimental results of P_{loss}/P_{in} for 3D-printed layers with thicknesses of 0.182 mm, 0.470 mm, and 0.986 mm are shown in Figure 5. The simulation results agree well with the experimental results.

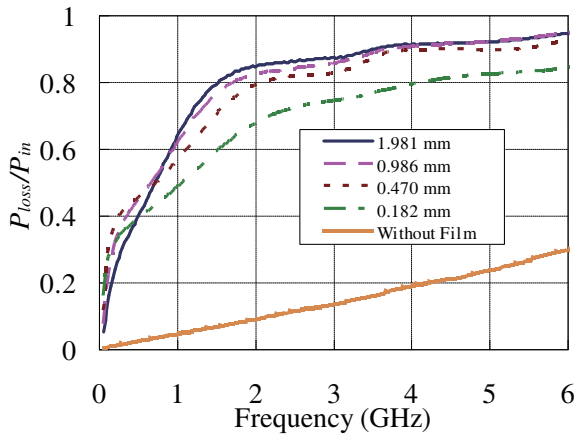

Figure 4. Frequency dependence of P_{loss}/P_{in} for 3D-printed layers with different measured thicknesses.

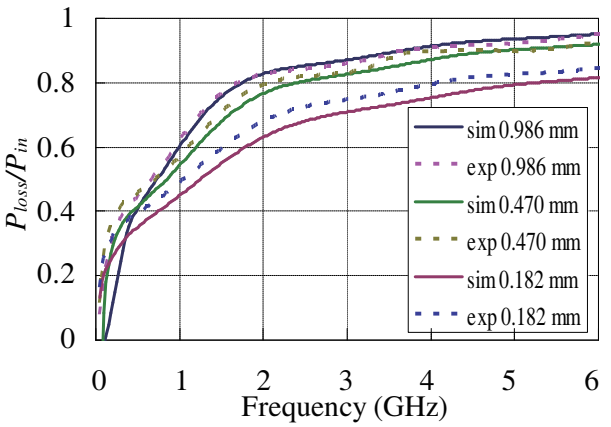

Figure 5. Simulation and experimental results of P_{loss}/P_{in} for 3D-printed layers with different thicknesses.

Table 3. Comparisons of films in terms of high-frequency power absorption.

Reference	Film	Process	P_{loss}/P_{in} (70% up)	Cost
[2]	ITO	Sputtering	1.5 GHz	High
[3]	Co-Al-O	Sputtering	2 GHz	High
[4]	Fe_3O_4	Sputtering	0.75 GHz	High
[5]	Co-Pd-Al-O	Sputtering	3 GHz	High
[14]	Carbon Black	Screen Printing	3 GHz	Low
Proposed	PLA + Carbon Black	3D-Printing	1.2 GHz	Low

Table 3 presents the power absorption characteristics of the 3D printed layer in this work in comparison with those reported in [2–5, 14]. In contrast to sputtering process, the proposed 3D printing process for the preparation of a power absorbing layer has the advantages of lower manufacturing cost and an easier process. In addition, the power absorption characteristics P_{loss}/P_{in} is greater than 70% measured at 1.2 GHz and is within the range of 80–95% measured in the frequency range of 2–6 GHz.

4. CONCLUSION

In this study, 3D printed PLA+carbon black-based layers are proposed for high-frequency power absorption on a microstrip line. The experimental results show that the absorption power is within the range of 80–95% in the frequency range of 2–6 GHz. The simulation results agree well with the experimental results. The 3D-printing technology enables the fast, economical, and environment friendly fabrication of power absorption layers. The results of this study can be applied to suppress noise that conducts through conductors in printed circuit board and in an RF transmission line.

REFERENCES

1. Ma, M. T. and M. Kanda, "Electromagnetic compatibility and interference metrology," *NASA STI/Recon Technical Report N*, Vol. 87, 16217, 1986.
2. Kim, S. H. and S. S. Kim, "Conduction noise absorption by ITO thin films attached to microstrip line utilizing Ohmic loss," *J. Appl. Phys.*, Vol. 108, No. 2, 024904, Jul. 2010.
3. Maruta, K., M. Sugawara, Y. Shimada, and M. Yamaguchi, "Analysis of optimum sheet resistance for integrated electromagnetic noise suppressors," *IEEE Trans. Magn.*, Vol. 42, No. 10, 3377–3379, Sep. 2006.
4. Kim, S. S., "Numerical analysis on power absorption by Fe_3O_4 thin films for conduction noise in microstrip line," *IEEE Trans. Magn.*, Vol. 48, No. 11, 3490–3493, Oct. 2012.
5. Ohnuma, S., H. Nagura, H. Fujimori, and T. Masumoto, "Noise suppression effect of nanogranular Co based magnetic thin films at gigahertz frequency," *IEEE Trans. Magn.*, Vol. 40, No. 4, 2712–2715, Aug. 2004.
6. Pissoort, D., J. Catrysse, T. Claeys, F. Vanhee, B. Boesman, and C. Brull, "Towards a stripline setup to characterise the effects of corrosion and ageing on the shielding effectiveness of EMI gaskets," *2015 IEEE International Symposium on Electromagnetic Compatibility (EMC)*, 7–12, Dresden, Germany, 2015.
7. Zeng, Z., Y. Yao, and Y. Zhuang, "A wideband common-mode suppression filter with compact-defected ground structure pattern," *IEEE Trans. Electromagn. Compat.*, Vol. 57, No. 5, 1277–1280, Jun. 2015.
8. Liu, Q., S. Connor, C. Olivieri, and F. D. Paulis, "Reduction of EMI due to common-mode currents using a surface-mount EBG-based filter," *IEEE Trans. Electromagn. Compat.*, Vol. 58, No. 5, 1440–1447, Jun. 2016.

9. Manzoor, Z., M. T. Ghasr, and K. M. Donnell, "Microwave characterization of 3D printed conductive composite materials," *2018 IEEE International Instrumentation and Measurement Technology Conference (I2MTC)*, 1–5, Houston, TX, 2018.
10. Viskadourakis, Z., K. C. Vasilopoulos, E. N. Economou, C. M. Soukoulis, and G. Kenanakis, "Electromagnetic shielding effectiveness of 3D printed polymer composites," *Appl. Phys. A*, Vol. 123, No. 12, 1–7, Nov. 2017.
11. Prince, T. J., E. J. Riley, and S. W. Miller, "Additive manufacturing of PLA-based microwave circuit-analog absorbers," *IEEE Trans. Electromagn. Compat.*, Vol. 63, No. 5, 1341–1346, 2021.
12. Lim, D., S. Yu, and S. Lim, "Miniaturized metamaterial absorber using three-dimensional printed stair-like Jerusalem cross," *IEEE Access*, Vol. 6, 43654–43659, 2018.
13. Chou, Y. J., L. S. Chen, and M. P. Houng, "High-frequency noise absorption of Ag-Fe_3O_4 films on microstrip transmission line," *IEEE Trans. Magn.*, Vol. 51, No. 4, 1–4, Jul. 2014.
14. Lin, G. S., J. L. Chen, L. S. Chen, and M. P. Houng, "Effect of carbon black film on high-frequency power absorption," *IEEE Microw. Wirel. Compon. Lett.*, Vol. 27, No. 9, 779–781, Aug. 2017.
15. Protopasta, https://www.proto-pasta.com/ (accessed Oct. 17, 2022).